UNCECOMP 2025
6th ECCOMAS Thematic Conference on
Uncertainty Quantification in Computational Sciences and Engineering
M. Papadrakakis, V. Papadopoulos, G. Stefanou (eds.)
Rhodes Island, Greece, 15–18 June 2025

UNCERTAINTY QUANTIFICATION OF WIRE TOLERANCES IN COIL ASSEMBLY

Romas Zubavicius[1], Maria Nogal[1], Gan Fu[2], Mitrofan Curti[2], Oswaldo Morales-Nápoles[1]

[1]Delft University of Technology
Delft, the Netherlands
{R.Zubavicius, M.Nogal, O.MoralesNapoles}@tudelft.nl

[2] Eindhoven University of Technology
Eindhoven, the Netherlands
{G.Fu, M.Curti}@tue.nl

Keywords: Uncertainty Quantification, Copula, Coreless Electric Motor, Coils, Multi-physics model

Abstract. *Manufacturing imperfections are an inherent aspect of the production process, affecting the reliability and performance of all engineered components, including actuators. This work investigates the effects of manufacturing uncertainty in coil assembly. Given the manufacturing tolerances of geometrical and material properties of wires and coils, the coil's electrical response is studied from a probabilistic perspective. While many researchers acknowledge these uncertainties, they often do not quantify their effects on the system's response. We propose the use of copulas to model nonlinear relationships and quantify the probabilistic dependence between design variables (i.e., wire and coil's properties) and their effects on electrical responses. Additionally, tolerances of the design variables are determined through unstructured expert elicitation. The results show the impact of the thickness of the wire's insulation in the performance of the coil. Furthermore, we establish a design space that is studied probabilistically, allowing for probabilistic design optimization.*

1 INTRODUCTION

Variations in manufacturing imperfections are expected during the manufacturing of coil assemblies used in actuators. The coil's electrical properties depend on the wire's geometrical and material parameters in addition to the coil's geometry, and its positioning with respect to the entire topology of the actuator. Consequently, many parameters, such as electrical properties, may vary between coils depending on the tolerances of the manufactured wire and coil assembly. Therefore, manufacturing tolerance is critical for the overall performance, reliability, and efficiency. However, achieving higher manufacturing precision leads to rapidly increasing costs and, beyond a certain level, such fine precision may become unnecessary depending on the specific application. Therefore, it is of interest to know what variables engineers have to consider when designing, manufacturing, and assembling devices to improve quality control.

Linear actuators are types of devices that produce force for a linear motion, i.e. to move objects in a straight line. Such devices are ubiquitous in various applications, from everyday uses, such as standing desks, to more industrial applications, such as assembly lines in manufacturing, to high-tech applications in scientific equipment, where precise movement control is in nanometers [1]. Achieving precise control requires the precise manufacturing and assembly of such devices. Probabilistic approaches to quantify uncertainties in the design stage can serve to improve quality control. More specifically, understanding the probabilistic dependencies between the variables involved in the manufacturing and assembly processes of linear actuators and studying how they affect the performance metrics help engineers to design devices under uncertainties and make improvements based on desired outcomes.

In this work, we aim to identify the probabilistic dependencies between the variables involved in the production of actuators, and how they can be characterized from a probabilistic point of view. More specifically, we study the dependence between design uncertainties, such as material properties, manufacturing and assembly tolerances, and how these uncertainties affect the performance of the actuator.

In actuator design, researchers often consider uncertainties but do not quantify their effects. Two common approaches to overcome the lack of uncertainty quantification are mentioned in [2] : i) designing under uncertainty using robust design optimization methods, in which the uncertainty characterization is captured by a range of uncertain conditions, and ii) avoiding certain manufacturing processes and opting for alternative designs that are less sensitive to uncertainties. On the other hand, the finite element method (FEM) is commonly employed to analyse the behaviour of actuator designs, which can be computationally intensive. This limits the number of uncertainties that can be studied. E.g., an article by Jiqi Wu et al. [3] only considered magnet material uncertainties. Similar approaches are found in [4, 5].

Uncertainty Quantification (UQ) methods vary from classical approaches, such as Monte Carlo (MC) simulations and Polynomial Chaos Expansion (PCE) to deep learning surrogate models [6]. While PCE can fall short due to orthogonal basis assumptions, and machine learning techniques are usually black boxes, copulas provide the advantage of having probabilistic interpretations, as well as their capability to model nonlinear relationships.

A general framework for UQ has been previously proposed using copulas [7], which considers complex input dependencies (e.g. multi-physics) via vine-copulas, as well as similar works which address multidimensional correlations [8]. While the frameworks exemplify methodologies on e.g. truss structures, or multiscale composite material, as per the authors' knowledge, it has never been applied to electric motors.

Existing methods for estimating uncertainties in manufacturing and assembly are often lim-

ited due to their dependence on complex processes, machine variability, and handling conditions. To address the challenge of acquiring uncertainties of manufacturing and assembly of actuators, we propose uncertainties of the design variables through expert elicitation. Furthermore, to expand on the proposed uncertainties, and quantify their effects, probabilistic dependencies were studied using copulas and the implications of these uncertainties were examined.

The remainder of the document is as follows; copulas are briefly introduced in Section 2. The multiphysics nature of actuators and the corresponding probabilistic modelling using copulas is explained in Section 3. The results are presented and discussed in Section 4, with concluding remarks in Section 5.

2 PROBABILISTIC DEPENDENCE VIA COPULAS

Copulas are flexible functions used to model multivariate probabilistic dependence [9]. The advantages of copulas become apparent for nonlinear relationships between random variables, because classical approaches, such as using multivariate normal distributions and Pearson correlation coefficients, fall short of explaining nonlinear behaviour. Copulas are prevalent in the finance sector [10], and in recent years, they have been applied more frequently to engineering problems [11]. The viability of copulas originates from Sklar's theorem [12], which states that for a joint distribution function H with margins F_i, there exists a copula C for all $(x_1, ..., x_d) \in \mathbb{R}^d$ such that

$$H(x_1, ..., x_d) = C(F_1(x_1), ..., F_d(x_d)) \tag{1}$$

The margins F_i are cumulative distribution functions (CDF), describing non-exceedance probability $F(x) = P(X \leq x)$. If the same underlying physics governs two systems, their dependence structure (and thus their copula) is likely to be similar. Therefore, system behaviour can be characterized via copulas. The common measure of dependence for copulas utilises rank correlations, which assess the relationship between variables based on their relative rankings within the dataset, rather than their values. In this work, Kendall's rank correlation (τ) [13], is used as a metric to check the significance of the bivariate distribution.

There are two common types of copula families - elliptical and Archimedean. Elliptical copulas are always symmetric. Archimedean copulas, on the other hand, can model various dependence structures, including some symmetries and tail dependencies. Tail dependence measures how strongly extreme values of random variables are correlated. Probabilistically, the upper tail (λ^U) and lower tail (λ^L) dependence coefficients are

$$\lambda^U = \lim_{t \to 1^-} P(X_1 > F_1^{-1}(t) \mid X_2 > F_2^{-1}(t)) \tag{2}$$

$$\lambda^L = \lim_{t \to 0^+} P(X_1 \leq F_1^{-1}(t) \mid X_2 \leq F_2^{-1}(t)) \tag{3}$$

defined as the limit (if it exists) for λ^U and λ^L as the conditional probability. It represents the asymptotic probability that X_1 is greater than the threshold $F_1^{-1}(t)$, given that X_2 is greater than $F_2^{-1}(t)$, as t approaches 1 from the left. Since t is arbitrarily close to 1 but never exactly 1, this captures the probability of extreme co-movements in the upper tail of the joint distribution. For lower tail dependence, it is the opposite, with the condition that is less than or equal to the quantile function evaluated at t, as t approaches 0 from the right. When $\lambda^U = \lambda^L = 0$, implies no tail dependence. Our work has two dominant types of copulas: Gaussian and Frank. These copulas are elliptic, have no tail dependence and are characterized by a single parameter.

Gaussian and Frank copulas are defined as

$$C_{\text{Gaussian}}(u, v; \rho) = \Phi(\Phi^{-1}(u), \Phi^{-1}(v); \rho). \tag{4}$$

$$C_{\text{Frank}}(u, v) = \frac{1}{\theta} \ln \left(1 + \frac{(e^{-\theta u} - 1)(e^{-\theta v} - 1)}{e^{-\theta} - 1} \right). \tag{5}$$

where for Gaussian copula, Φ^{-1} is the inverse of standard normal CDF, and the dependence between two variables is controlled by correlation coefficient ρ. The dependence in Frank copula is described by parameter θ, with $\theta > 0$ indicating a positive relationship, and $\theta < 0$ negative. Similar to the Gaussian copula, it has symmetric dependence, however, it captures strong central dependence and weaker dependence in its tails. To facilitate a more intuitive interpretation of the dependence structure, the copula unit space (u, v) is transformed into standard normal space (z_u, z_v). This transformation is achieved by applying the inverse CDF of the standard normal distribution. It is defined as $z_u = \Phi^{-1}(u)$ and $z_v = \Phi^{-1}(v)$, where u and v are uniform $[0, 1]$ variates. If u and v originate from a Gaussian copula, the transformed plot will exhibit characteristics consistent with the bivariate normal. The visualization of the Gaussian copula in unit space is shown in Figure 1a, and the standardized copula is shown in Figure 1b, and Frank copula is shown in Figure 2a, and in standard normal space Figure 2b.

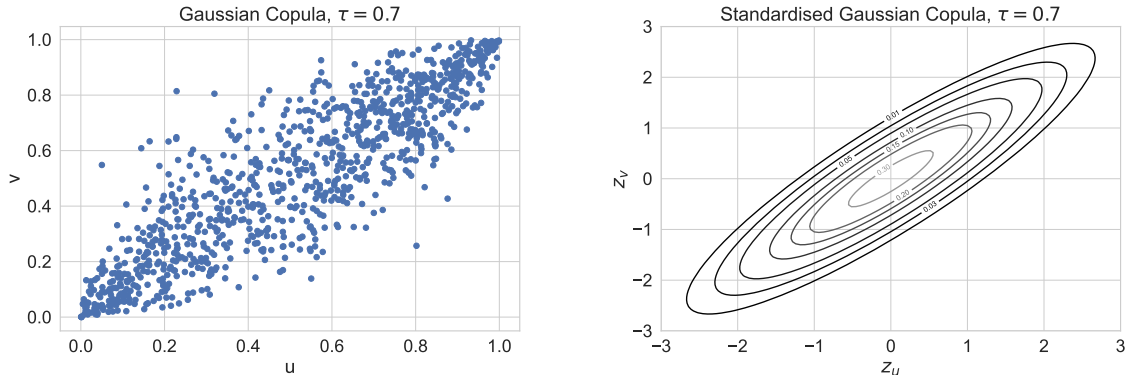

(a) (b)

Figure 1: Bivariate Gaussian copula of (u, v) with Kendall $\tau = 0.7$ in (a) unit space, and (b) standard normal space.

3 PHYSICAL MODEL OF THE ACTUATOR

The actuator under study is a Permanent Magnet Linear Synchronous Motor (PMLSM) with a single-sided permanent magnet (PM) configuration as depicted in Figure 3.

It employs rectangular wire for the winding. It features a configuration of four magnets, three coils, and six stacks. Each coil is wound with 261 wire turns while stacking refers to the arrangement of multiple coils positioned on top of one another. For an application-specific case, a 10 kg load is assumed for the motor. This case has been selected because mechanical performance, such as force ripples are less present in coreless motors; however, manufacturing tolerances are relatively more significant. The design variables and the associated uncertainties and the multiphysics model used to study this case are described in subsequent sections.

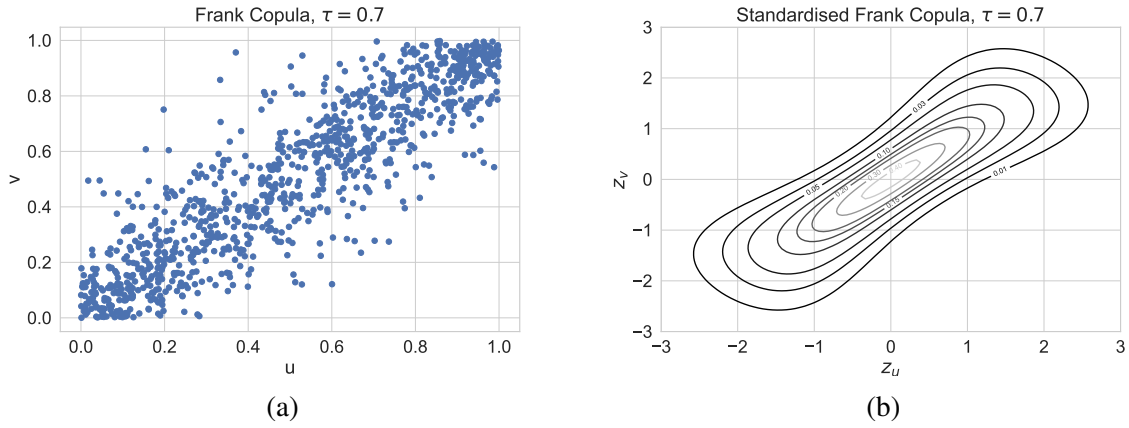

Figure 2: Bivariate Frank copula of (u, v) with Kendall $\tau = 0.7$ in (a) unit space, and (b) standard normal space.

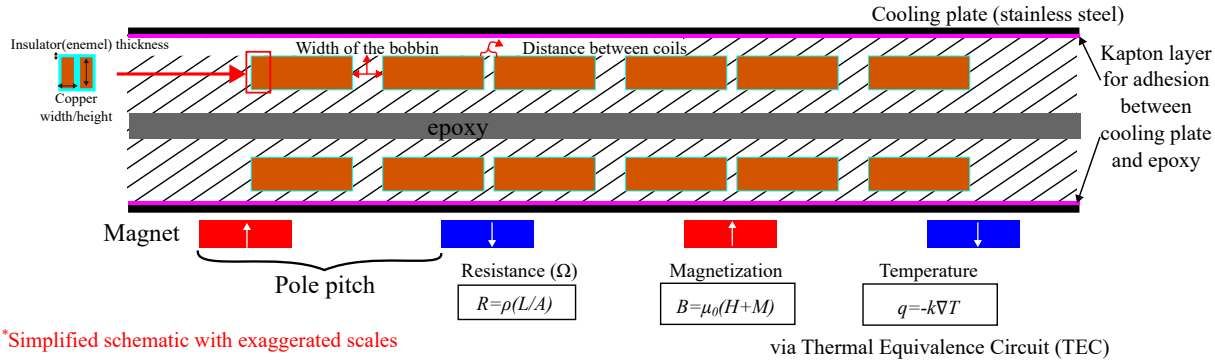

Figure 3: Illustration of a cross-section of a coreless linear motor, with 4 magnets and 3 coils. Epoxy is filled and encapsulates the coils. Each coil has 261 turns and is a 6-stack configuration.

3.1 Design variables of the actuator

The initial design variables are acquired from [14] and adjusted for high-voltage applications, resulting in a set of 20 input variables. Their description and uncertainty characterization are indicated in Table 1. Out of the 20 input variables, 18 are considered random variables. The exceptions are the air gap length between the coil and PM due to complex dependencies on the tolerances of epoxy and cooling plates. The rectangular part has a strong influence on the force, but is considered to be invariant, because the manufacturing tolerance is considered to reflect on the bent part, which considered has no contribution to the force.

The uncertainties presented in the table define the lower and upper bounds. Since obtaining precise uncertainty estimates is challenging, the uncertainty bounds were acquired through expert elicitation, by sending a questionnaire to experts with the design variables, and requesting their estimates of expected deviations. The generalized Beta distribution is used for the majority of the variables as it offers the advantage of being bounded and allows for nonsymmetric distributions. The Beta probability distribution function is defined on the interval $[0, 1]$, meaning that the random variable $X \sim GBeta(\alpha, \beta, x_L, x_U)$ defined in the range $[x_L, x_U]$ has to be transformed into the variable $Z \sim Beta(\alpha, \beta)$ through an affine transformation. Thus, $Z = \frac{X - x_L}{x_U - x_L}$. The uncertainty distributions are assumed to be symmetric, hence the shape parameters were chosen to be equal, resulting in a Gaussian shape distribution, with the advantage of being bounded. Given that the distributions depend on the manufacturing pro-

cesses, which are difficult to describe [2], the parameters of the beta distributions are assumed $\alpha = \beta = 7.5$. This choice should be validated. These parameters result in Beta distributions with $E[Z] = 0.5$ and standard deviation $\sigma_Z = 0.125$, which transformed to the original variable results in $E[X] = \frac{x_U + x_L}{2}$ and $\sigma_X = \frac{x_U + 7x_L}{8}$, respectively. Uniform distributions were chosen to represent less well-defined uncertainties.

Design variable [units]	Expected value	Support range	Probability Distribution
Width wire [mm]	0.06	$\pm$2%	GBeta
Height wire [mm]	1.27	$\pm$2%	GBeta
Thickness insulation [mm]	0.015	$\pm$10%	Uniform
Pole pitch [mm]	42	$\pm$1%	GBeta
Length rect. part [mm]	70	-	Deterministic
Radius of bobbin [mm]	4	$\pm$1 turn thickness	GBeta
Height of PM [mm]	10	$\pm$0.1 mm	GBeta
Length of PM [mm]	70	$\pm$0.15 mm	GBeta
Height stainless steel [mm]	0.25	$\pm$1%	GBeta
Height epoxy layer [mm]	0.2	$\pm$2.5%	GBeta
Height cooling plate [mm]	1	$\pm$1%	GBeta
Height kapton [mm]	0.05	$\pm$12 μm	GBeta
Distance between coils [mm]	1	$\pm$1 turn thickness	GBeta
Airgap length [mm]	0.5	-	Deterministic
Density epoxy [kg/m^3]	1300	$\pm$10%	Uniform
Density steel [kg/m^3]	8000	$\pm$0.3%	GBeta
Specific heat capacity epoxy [J/(kg°C)]	1100	$\pm$10%	Uniform
Thermal cond. epoxy [W/(mk)]	1.2	$\pm$20%	Uniform
Resistivity [$\Omega \cdot \mathrm{m}$]	1.724e-8	$\pm$0.5%	Uniform
Remanence [T]	1.23	$\pm$3%	GBeta

Table 1: Set of design and material properties used to run the simulation. Uncertainty of the variables was acquired via unstructured expert elicitation.

3.2 Multiphysics model of the actuator

A comprehensive multi-physics model has been developed as a design tool for actuator topology optimization. This model evaluates actuator performance across various topologies under a given motion profile and mass load. It integrates electrical, magnetic, mechanical, and thermal behaviours to achieve a thorough assessment. The design illustration can be seen in Figure 3.

For clarity, the model is structured into three main components: Inputs, Physical Models, and Outputs.

1) In the inputs block: we pre-define the geometric dimensions of the components of the actuator, namely, wire's height, thickness, with a certain thickness of enamel layer; number of turns for one coil; stacks of coils for one phase; together with the dimension of the epoxy potting layer, Kapton insulation layer, and the stainless steel cooling plates. In addition to the geometric structures, the environmental conditions and the materials' properties are predefined in this block. Most importantly, the fourth-order (position, velocity, jerk and snap) motion profile (shown in Figure 4a) and mass load are prescribed.

2) The core of the model is the multi-physics model. First, the prescribed motion profile dictates the mechanical requirements, enabling the evaluation of force density, motor constant, and different voltage components (seen in Figure 4b), which are inherently coupled with electrical excitations and magnetic field modeling. Second, a harmonic modelling technique based on Fourier analysis [15, 16] is employed to solve the 2D magnetic field distribution of the actuator, considering the structure of PMs and coils. Additionally, the inductance of the winding is modelled by analyzing the flux linkage induced by a unified single-phase current excitation, enabling precise calculation of inductive voltage components. Lastly, a 3D thermal equivalent circuit (TEC) [17] is implemented to predict the thermal behaviour of the system. This thermal model is coupled with the copper losses, determined by the computed three-phase current required to achieve the motion profile. Notably, the TEC model accounts for the bent geometry of the coils and their anisotropic thermal conductivity.

3) The model generates a diverse set of performance metrics, including fill factor; force density; steepness; motor constant; and terminal voltage, which includes Electromotive force (EMF) as well as resistive and inductive voltage components; phase currents; power consumption (copper losses and mechanical output); magnetic field distribution; and coil/insulation temperatures, etc. These outputs facilitate a comprehensive evaluation of different topological designs and aid in assessing the impact of uncertainties on actuator performance.

3.3 Performance metrics of the actuator

As mentioned in the previous section, several performance metrics are defined to evaluate the motor design: namely voltage, force density, power density, motor constant, fill factor, and temperature (calculated via TEC).

3.3.1 Voltage

Voltage calculations are based on the motion profile (as seen in Figure 4). The total voltage

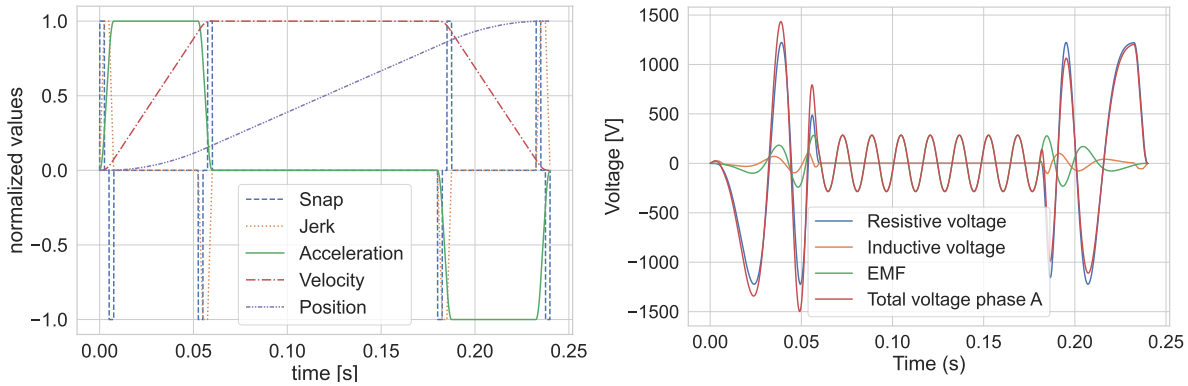

(a) (b)

Figure 4: Required voltage is obtained based on motion profile. (a) Motion profile; (b) Voltage of a single phase

has three components: resistive, inductive, and electromotive force (EMF), for each of the three phases. The equation associated with one of the phase voltages is as follows:

$$V_{\text{an}} = I_a R_a + L_{aa}\frac{dI_a}{dt} + M_{ab}\frac{dI_b}{dt} + M_{ac}\frac{dI_c}{dt} + E_a \tag{6}$$

where the first component ($I_a R_a$) is the resistive voltage, three inductive voltages with (L_{aa}) self-inductance, and (M_{aa}, M_{ab}) mutual inductances and the EMF component (E_a) which is proportional with the speed of the mover. Subscripts a, b, c signify the three-phase electrical system. The EMF equation is given as

$$E_n = \frac{\partial \lambda_{\mathrm{n,pm}}}{\partial t} = \frac{\partial \lambda_{\mathrm{n,pm}}}{\partial x}\frac{\partial x}{\partial t} = \frac{\partial \lambda_{\mathrm{n,pm}}}{\partial x}\nu \tag{7}$$

where λ is the flux linkage in one phase, which is calculated from the 2D harmonic model.

3.3.2 Force density

Force density quantifies the force per unit volume of the actuator and is defined as

$$\text{Force density} = \frac{F}{V_{\mathrm{vol}}}, \tag{8}$$

where F is the force exerted by the actuator, calculated as the product of its mass and the acceleration derived from the motion profile, plus the friction force.

3.3.3 Power density

Similar to force density, power density describes the power output relative to volume and is given by

$$\text{Power density} = \frac{I \cdot V_{\mathrm{tot}}}{V_{\mathrm{vol}}}. \tag{9}$$

3.3.4 Motor constant

The motor constant is given by the ratio F/I. It quantifies how much force the actuator generates with a unit current excitation. Force is position independent, linear with current, and maximized if $\theta_0 = 90$. Therefore, it can expressed as follows

$$F_x = \sum_{n=a,b,c} \frac{E_n I_n}{\nu} = \frac{3\pi}{2\tau}\lambda_{\mathrm{pm}} I \sin(\theta_0) = K_t I \sin(\theta_0) \tag{10}$$

where K_t is the motor constant, and θ is the commutation angle, which is the phase shift between the magnet's magnetic field and the coil's magnetic field.

3.4 Filling factor

The filling factor is another key design variable used in the design considerations, affecting thermal management and electrical performance

$$\text{Filling Factor} = \frac{A_{\mathrm{conductor}}}{A_{\mathrm{total}}} \tag{11}$$

where $A_{\mathrm{conductor}}$ is the conductor cross-sectional area. It is calculated as the ratio of the conductor to the total available area, which includes enamel.

3.5 Probabilistic modelling

The multiphysics simulation was executed for 60,000 iterations, with each iteration sampling variables from the predefined probability distributions, following a standard Monte Carlo approach. All simulation data were stored in a CSV file, including the sampled design variables and the corresponding results. Bivariate copulas were fitted to the data to analyze the dependence structure between inputs and outputs. The fitting was performed using pyvinecopulib [18]. The following copulas with rotations were analyzed: Gaussian, Student, Clayton, Gumbel, Frank, BB1, BB6, BB7, BB8. The most appropriate copula model was selected based on the Akaike Information Criterion (AIC) because it penalizes overfitting, and allows a fair comparison between models.

4 RESULTS & DISCUSSION

This section presents the results of bivariate probabilistic modelling. Section 4.1 discusses the results between inputs and outputs of the model and Section 4.2 discusses dependencies between outputs, studying the design space probabilistically.

4.1 Dependencies between design variables and performance metrics

Small uncertainties in the assembly and material properties propagate and amplify in the performance of the manufactured component. For example, the variability ranges observed in the input parameters result in voltage peaks ranging from 1342 V at the 5th percentile to 1639 V at the 95th percentile, and temperature ranging from 82 °C at the 5th percentile to 114 °C, 95th percentile, as shown in Figure 5.

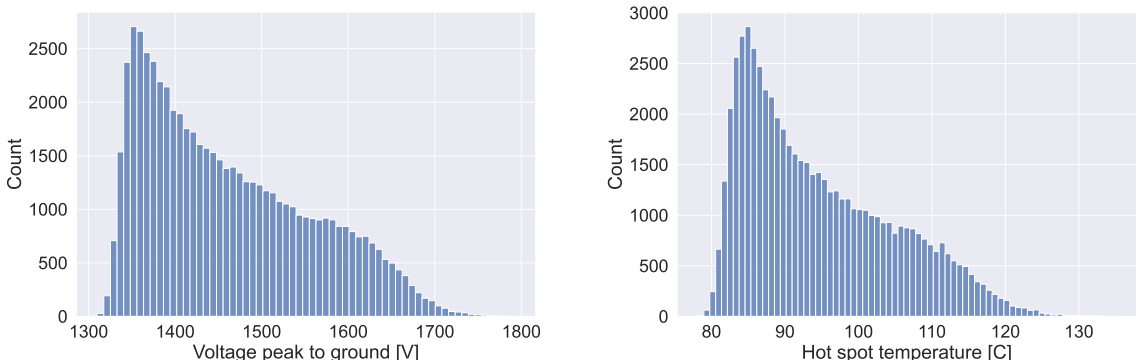

(a) (b)

Figure 5: Multiphysics model outputs distributions shown in (a) voltage, and (b) temperature

The bivariate distributions between the inputs (design variables) and outputs (simulation results) reveal that the wire insulation thickness is the most significant input variable, as it shows the highest rank correlation with voltage. On the other hand, the coil width, which is a latent variable determined by the wire's geometric properties, exhibits the highest rank correlation with the same variable. The best-fitted copula between the thickness of insulation and all performance metrics is the frank copula, indicating a stronger correlation at the median, i.e., values closer to the reference design. The standardised scatter plot of the data transformed to standard normal, along with the standard normal transformation of the fitted copula contour

plot is shown in Figure 6a. The insulation thickness affects the geometrical properties of the assembled coil, such as its width and height, and this insulation significance is apparent for the effective coil dimensions (as seen in Figure 6b). The significance of insulation thickness, for performance and reliability is further highlighted in [19]

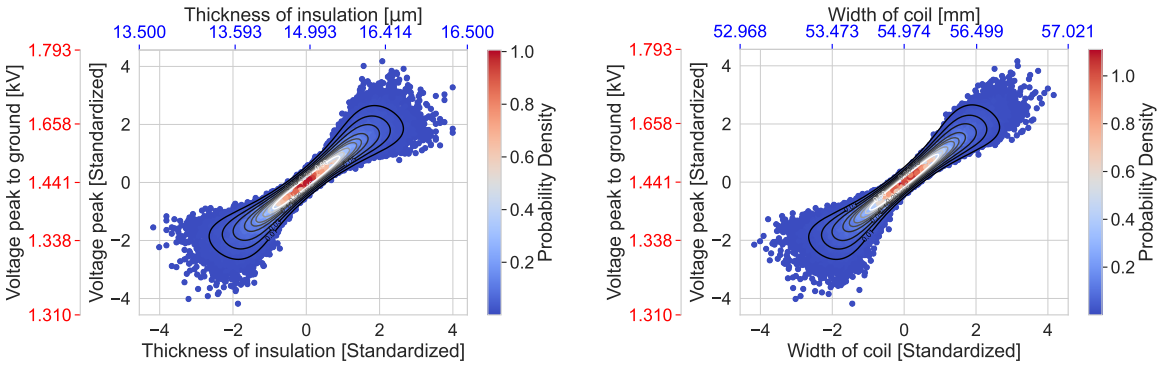

(a) (b)

Figure 6: Standardized copula results between (a) thickness of wire insulation and voltage, and (b) width of the coil and voltage. In standard axes, the median value is at (0,0). The contour plot is shown directly from the fitted copula.

Some of the design variables do not show a strong dependence under the defined uncertainties. For example, variations in the thermal conductivity of epoxy exhibit a weak correlation with the analysed performance metrics, such as temperature (see Figure 7a). However, two

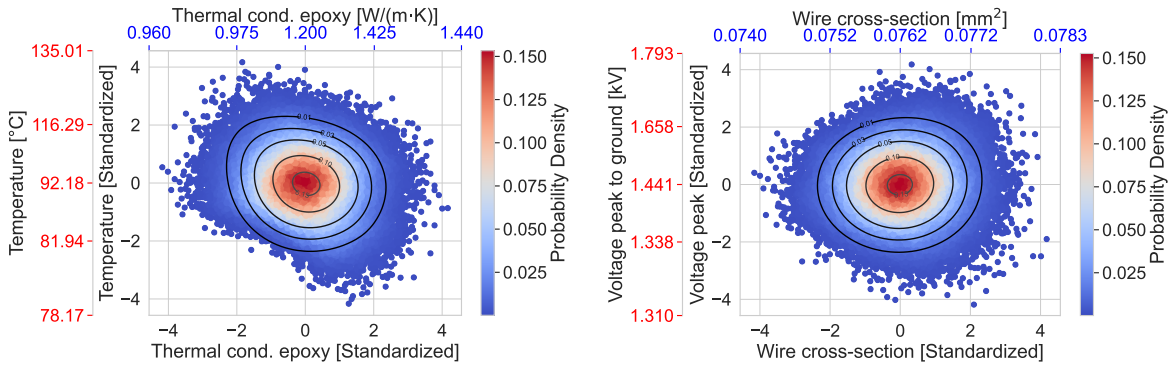

(a) (b)

Figure 7: Standardized copula between (a) thermal conductivity of the epoxy and temperature and (b) cross-sectional area of the wire and voltage. In standard axes, the median value is at (0,0). The contour plot is shown directly from the fitted copula.

regions of interest can be identified: lower temperatures are not achievable at lower thermal conductivities, indicating that epoxy thermal resistance (proportional inverse to the thermal conductivity) is more significant in the system design. Conversely, at higher thermal conductivities, the thermal resistance from the epoxy becomes less dominant, allowing for better cooling. This illustrates a clear example of a probabilistic design space, where possible designs can be

probabilistically determined under uncertainties. Similarly, in contrast to the wire insulation, the cross-sectional area of the wire does not exhibit a strong correlation to any of the performance metrics, see Figure 7b. This relationship has a weak tail dependence, at lower cross-sectional area, the voltage variations are relatively smaller, compared to higher cross-sectional area. Design variables such as the bobbin radius, PM length, stainless steel height, PM height, Kapton height, epoxy layer height, cooling plate height, coil spacing, density, and specific heat capacity generally do not exhibit strong bivariate dependence on the performance metrics (see Tables 2 in the appendix). While wire resistivity does impact the total resistance, its influence is less significant compared to the geometric parameters.

4.2 Dependencies between performance metrics

The performance metrics describe the motor's efficiency. Analyzing the dependencies between performance metrics, such as voltage, temperature and motor constant allows defining the probabilistic design space. The probabilistic design space describes, for instance, under which voltage or what temperature ranges can be achieved from a probabilistic view.

In our case study, an important consideration is that this study focuses solely on uncertainties by introducing small variations in the design variables and analyzing their effects. If the design space were expanded, i.e. different topologies of the actuator were considered, the bivariate dependence could change due to nonlinear physical behaviour emerging at different parameter ranges. Nevertheless, several key insights are gained. An interesting tail dependence between voltage and motor constant has been observed. Figure 8a shows that at low voltages, higher motor constants are achieved, the inherent reason for this is that optimal design requires less current to achieve the same force and motion profile, which leads to higher motor constant and lower voltage, that's why we see the low voltage is highly correlated with higher motor constant. Vice versa for the high voltage-low K_t; however, the motor constant presents more variability in these range of values (upper left side of the figure). It is also observed that the expected design variables are still strongly correlated (central part of the figure), exhibiting very small variations in performance metrics, as explained in the previous section. When these optimal geometric proportions are altered, the motor constant deviates more significantly from expected values, resulting in increased variability, however, with a strong dependence showing motor inefficiency (lower right side of the figure).

Relatively similar results can be observed with temperature, showing that a higher required voltage also results in a higher temperature of the motor (Figure 8b). Interestingly, frank copula, which has no tail dependence has a better fit than other copulas with tail dependences based on the AIC. The lower and median voltage values exhibit similar temperature behaviour to the motor constant; however, the upper tail seemingly has more spread than the motor constant did. Table 3 in the appendix summarizes bivariate dependencies between performance metrics.

5 CONCLUSIONS & FUTURE WORK

In this paper, the propagation of the uncertainties associated with manufacturing, assembly and material properties to the performance metrics of a coreless linear motor are quantified with probabilistic methods. First, expert elicitation is performed to estimate design uncertainties, and probability distributions are defined. Secondly, a standard Monte Carlo approach is utilised with 60,000 runs of a multiphysics model of the coreless linear motor capturing the interdependencies between electrical, mechanical, magnetic and thermal behaviours. Then, bivariate copulas are fitted between the inputs and outputs of the model, quantifying the bivariate probabilistic

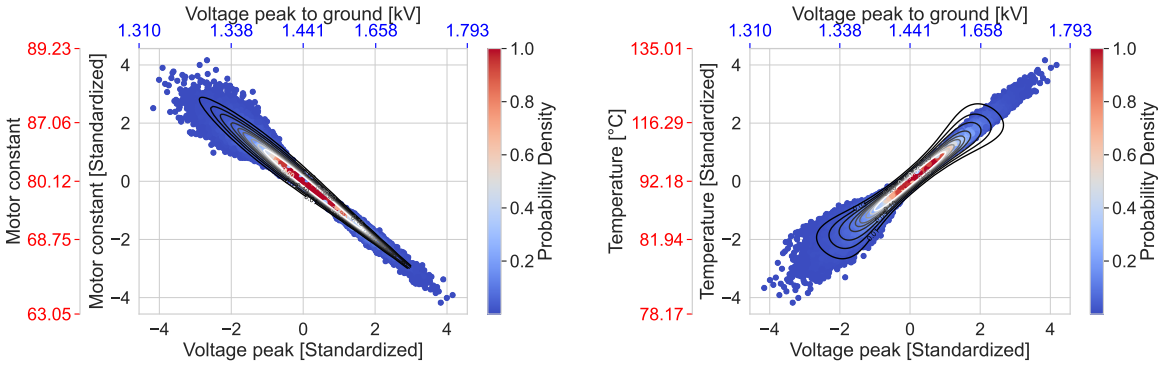

(a) (b)

Figure 8: Probabilistic design space given by the standardized copula between (a) voltage and motor constant and (b) voltage and temperature. In standard axes, the median value is at (0,0). The contour plot is shown directly from the fitted copula. Figure a) shows motor inefficiency, by requiring higher voltage for the same application, and b) shows the temperature increase with higher voltage.

relationship and mapping the probabilistic design space. The results show that the uncertainty of the thickness of insulation plays the most important role in the design of the coreless linear motor. By increasing insulation thickness, it increases the mass of the actuator, while also affecting the ratios between the width of the coil and magnet, decreasing the overall efficiency. Other dependence structures, such as the bivariate copula between the thermal conductivity of the epoxy and temperature or the copula between the cross-sectional area of the wire and voltage do not show a dominant dependence under uncertainties; However, the scatter plots reveal regions of interest, indicating ranges of possible design configurations where performance metrics exhibit favorable characteristics or heightened sensitivity to specific parameter variations. Tables 2 and 3 in the appendix summarize all bivariate dependencies indicating the best-fit copula and rank correlation. The color scheme ranges from green, indicating a positive correlation, to red, representing a negative correlation. Text in bold highlights the discussed copulas in this paper. There are several limitations to this work. To manufacture and assemble these actuators is very costly, limiting the validation of these results. If we consider validation with only the coils, this would imply completely different assumptions, which would be invalid for this case study. Additionally, only a bivariate case was considered, which does not capture complex dependencies between multiple variables. Vine-copulas could be considered for multi-physics case studies.

REFERENCES

[1] Awaddy, B.A. and Wu-Chu Shih and Auslander, D.M., *Nanometer Positioning of a Linear Motion Stage under Static Loads*. IEEE/ASME Transactions on Mechatronics, 113-119.

[2] Y. Cheng, L. Ding, T. Zhao and S. Cui, *Design and Optimization of Electric Vehicle Traction Motor Considering Rotor Topology and Manufacturing Uncertainty* in IEEE Transactions on Industrial Electronics, vol. 71, no. 5, pp. 5034-5044

[3] J. Wu, X. Zhu, D. Fan, Z. Xiang, L. Xu and L. Quan, *Robust Optimization Design for Permanent Magnet Machine Considering Magnet Material Uncertainties,* in IEEE Transactions on Magnetics, vol. 58, no. 2, pp. 1-7,

[4] P. Offermann, H. Mac, T. T. Nguyen, S. Clénet, H. De Gersem and K. Hameyer, *Uncertainty Quantification and Sensitivity Analysis in Electrical Machines With Stochastically Varying Machine Parameters*, in IEEE Transactions on Magnetics, vol. 51, no. 3, pp. 1-4,

[5] V. Rafiee and J. Faiz, *Uncertainty Quantification of Permanent Magnet Motor Using Response Surface Surrogate Modeling,* 2020 11th Power Electronics, Drive Systems, and Technologies Conference (PEDSTC), Tehran, Iran, 2020, pp. 1-5

[6] M. Abdar, F. Pourpanah, S. Hussain, D. Rezazadegan, L. Liu, M. Ghavamzadeh, P. Fieguth, X. Cao, A. Khosravi, U. R. Acharya, V. Makarenkov, and S. Nahavandi *A review of uncertainty quantification in deep learning: Techniques, applications and challenges*

[7] Emiliano Torre and Stefano Marelli and Paul Embrechts and Bruno Sudret, *A general framework for data-driven uncertainty quantification under complex input dependencies using vine copulas*, Probabilistic Engineering Mechanics, 1-16

[8] Xu, C., Zhu, P., Liu, Z., & Tao, W. (2020). *Mapping-Based Hierarchical Sensitivity Analysis for Multilevel Systems With Multidimensional Correlations.* Journal of Mechanical Design, 143(1). https://doi.org/10.1115/1.4047689

[9] Nelsen, R. B. *An introduction to copulas.* springer.

[10] Jondeau, Eric, and Michael Rockinger. *The copula-garch model of conditional dependencies: An international stock market application.* Journal of international money and finance 25.5 (2006): 827-853

[11] B. Renard, M. Lang, *Use of a Gaussian copula for multivariate extreme value analysis: Some case studies in hydrology* Advances in Water Resources 897-912

[12] A. Sklar, *Fonctions de r ´epartition 'a n dimensions et leurs marges*, Publ. Inst. Statist. Univ. Paris 8 (1959) 229–231.

[13] Kendall, Maurice G. *"A new measure of rank correlation." Biometrika 30.1-2 (1938): 81-93.*

[14] van Beek, T. A. *Towards high voltage in coreless linear motors : solutions to thermal and electric-field problems in high force-density applications.* [Phd Thesis 1 (Research TU/e / Graduation TU/e), Electrical Engineering]. Technische Universiteit Eindhoven.

[15] Gysen, B. L. J., Meessen, K. J., Paulides, J. J. H. and Lomonova, E. A. [2010b], *General formulation of the electromagnetic field distribution in machines and devices using Fourier analysis*. IEEE Transactions on Magnetics 46(1), 39–52.

[16] Gysen, B. L. J., Ilhan, E., Meessen, K. J., Paulides, J. J. H. and Lomonova, E. A. [2010a], *Modeling of flux switching permanent magnet machines with Fourier analysis*, IEEE Transactions on Magnetics 46(6), 1499–1502.

[17] G. Fu, M. Curti and E. Lomonova, *Anisotropic 3-D Thermal Modeling for a Racetrack Foil Coil*, 2024 IEEE 21st Biennial Conference on Electromagnetic Field Computation-Extended Papers (CEFC-Extended), Jeju, Korea, Republic of, 2024, pp. 1-4, doi: 10.1109/CEFC65091.2024.10848784.

[18] Nagler, T. and T. Vatter. *pyvinecopulib (v0.7.0).* Zenodo. https://doi.org/10.5281/zenodo.14616803

[19] L. V. Hanisch, J. Franzki and M. Henke, *Impact of Insulation and Cooling on Performance due to Reliability-Oriented Design of Electrical Machines,* 2022 24th European Conference on Power Electronics and Applications (EPE'22 ECCE Europe), Hanover, Germany, 2022, pp. 1-7.

APPENDIX

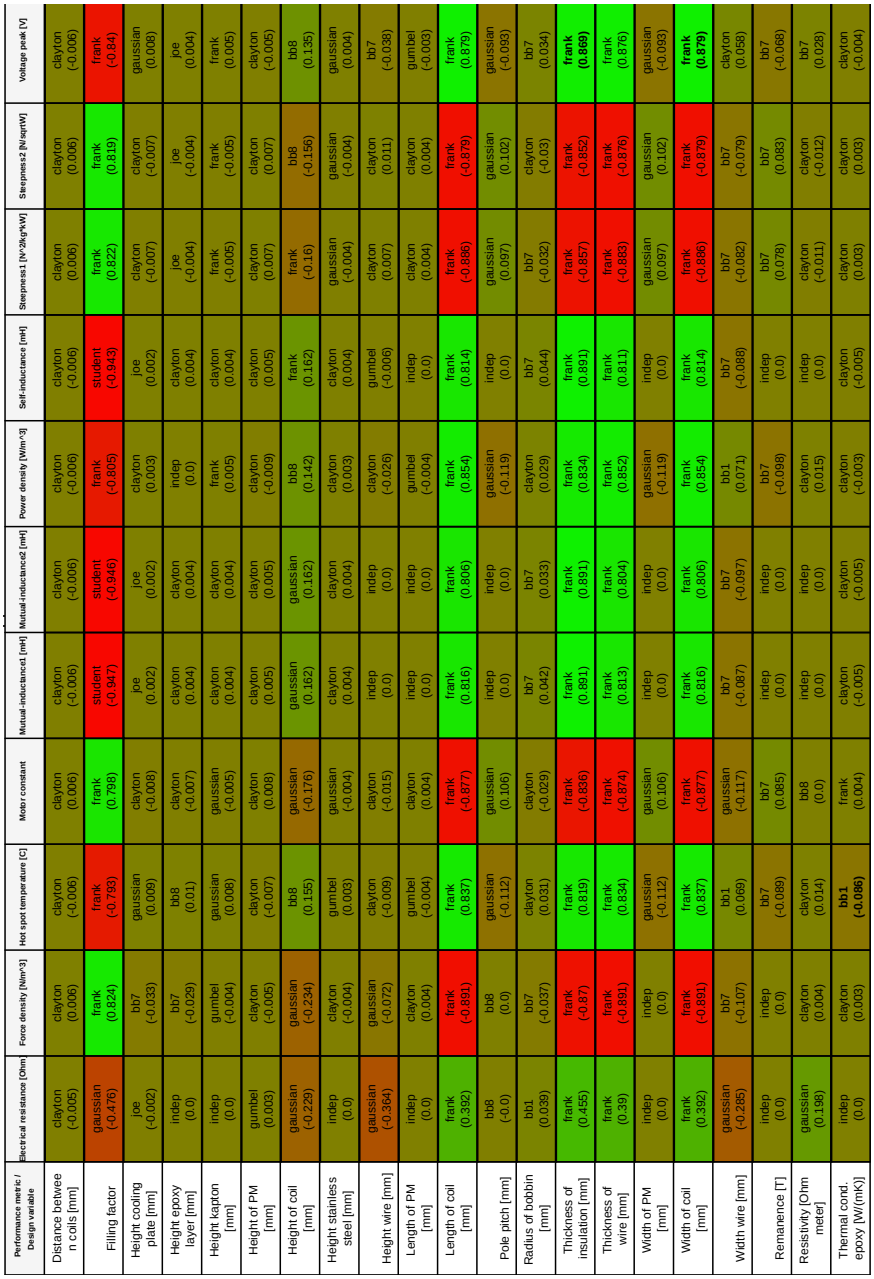

Performance metric / Design variable	Electrical resistance [Ohm]	Force density [N/m^3]	Hot spot temperature [C]	Motor constant	Mutual-inductance1 [mH]	Mutual-inductance2 [mH]	Power density [W/m^3]	Self-inductance [mH]	Steepness1 [N^2/kg*W]	Steepness2 [N/sqrtW]	Voltage peak [V]
Distance between coils [mm]	clayton (-0.005)	clayton (0.006)	clayton (-0.006)	clayton (0.006)	clayton (-0.006)	clayton (-0.006)	clayton (-0.006)	clayton (-0.006)	clayton (0.006)	clayton (0.006)	clayton (-0.006)
Filling factor	gaussian (-0.476)	frank (0.824)	frank (-0.793)	frank (0.798)	student (-0.947)	student (-0.946)	frank (-0.805)	student (-0.943)	frank (0.822)	frank (0.819)	frank (-0.84)
Height cooling plate [mm]	joe (-0.002)	bb7 (-0.033)	gaussian (0.009)	clayton (-0.008)	joe (0.002)	joe (0.002)	clayton (0.003)	joe (0.002)	clayton (-0.007)	clayton (-0.007)	gaussian (0.008)
Height epoxy layer [mm]	indep (0.0)	bb7 (-0.029)	bb8 (0.01)	clayton (-0.007)	clayton (0.004)	clayton (0.004)	indep (0.0)	clayton (0.004)	joe (-0.004)	joe (-0.004)	joe (0.004)
Height kapton [mm]	indep (0.0)	gumbel (-0.004)	gaussian (0.008)	gaussian (-0.005)	clayton (0.004)	clayton (0.004)	frank (0.005)	clayton (0.004)	frank (-0.005)	frank (-0.005)	frank (0.005)
Height of PM [mm]	gumbel (0.003)	clayton (-0.005)	clayton (-0.007)	clayton (0.008)	clayton (0.005)	clayton (0.005)	clayton (-0.009)	clayton (0.005)	clayton (0.007)	clayton (0.007)	clayton (-0.005)
Height of coil [mm]	gaussian (-0.229)	gaussian (-0.234)	bb8 (0.155)	gaussian (-0.176)	gaussian (0.162)	gaussian (0.162)	bb8 (0.142)	frank (0.162)	frank (-0.16)	bb8 (-0.156)	bb8 (0.135)
Height stainless steel [mm]	indep (0.0)	clayton (-0.004)	gumbel (0.003)	gaussian (-0.004)	clayton (0.004)	clayton (0.004)	clayton (0.003)	clayton (0.004)	gaussian (-0.004)	gaussian (-0.004)	gaussian (0.004)
Height wire [mm]	gaussian (-0.364)	gaussian (-0.072)	clayton (-0.009)	clayton (-0.015)	indep (0.0)	indep (0.0)	clayton (-0.026)	gumbel (-0.006)	clayton (0.007)	clayton (0.011)	bb7 (-0.038)
Length of PM [mm]	indep (0.0)	clayton (0.004)	gumbel (-0.004)	clayton (0.004)	indep (0.0)	indep (0.0)	gumbel (-0.004)	indep (0.0)	clayton (0.004)	clayton (0.004)	gumbel (-0.003)
Length of coil [mm]	frank (0.392)	frank (-0.891)	frank (0.837)	frank (-0.877)	frank (0.816)	frank (0.806)	frank (0.854)	frank (0.814)	frank (-0.886)	frank (-0.879)	frank (0.879)
Pole pitch [mm]	bb8 (-0.0)	bb8 (0.0)	gaussian (-0.112)	gaussian (0.106)	indep (0.0)	indep (0.0)	gaussian (-0.119)	indep (0.0)	gaussian (0.097)	gaussian (0.102)	gaussian (-0.093)
Radius of bobbin [mm]	bb1 (0.039)	bb7 (-0.037)	clayton (0.031)	clayton (-0.029)	bb7 (0.042)	bb7 (0.033)	clayton (0.029)	bb7 (0.044)	bb7 (-0.032)	clayton (-0.03)	bb7 (0.034)
Thickness of insulation [mm]	frank (0.455)	frank (-0.87)	frank (0.819)	frank (-0.836)	frank (0.891)	frank (0.891)	frank (0.834)	frank (0.891)	frank (-0.857)	frank (-0.852)	**frank (0.869)**
Thickness of wire [mm]	frank (0.39)	frank (-0.691)	frank (0.834)	frank (-0.874)	frank (0.813)	frank (0.804)	frank (0.852)	frank (0.811)	frank (-0.883)	frank (-0.876)	frank (0.876)
Width of PM [mm]	indep (0.0)	indep (0.0)	gaussian (-0.112)	gaussian (0.106)	indep (0.0)	indep (0.0)	gaussian (-0.119)	indep (0.0)	gaussian (0.097)	gaussian (0.102)	gaussian (-0.093)
Width of coil [mm]	frank (0.392)	frank (-0.891)	frank (0.837)	frank (-0.877)	frank (0.816)	frank (0.806)	frank (0.854)	frank (0.814)	frank (-0.886)	frank (-0.879)	**frank (0.879)**
Width wire [mm]	gaussian (-0.285)	bb7 (-0.107)	bb1 (0.069)	gaussian (-0.117)	bb7 (-0.087)	bb7 (-0.097)	bb1 (0.071)	bb7 (-0.088)	bb7 (-0.082)	bb7 (-0.079)	clayton (0.058)
Remanence [T]	indep (0.0)	indep (0.0)	bb7 (-0.089)	bb7 (0.085)	indep (0.0)	indep (0.0)	bb7 (-0.098)	indep (0.0)	bb7 (0.078)	bb7 (0.083)	bb7 (-0.068)
Resistivity [Ohm meter]	gaussian (0.198)	clayton (0.004)	clayton (0.014)	bb8 (0.0)	indep (0.0)	indep (0.0)	clayton (0.015)	indep (0.0)	clayton (-0.011)	clayton (-0.012)	bb7 (0.028)
Thermal cond. epoxy [W/(mK)]	indep (0.0)	clayton (0.003)	**bb1 (-0.086)**	frank (0.004)	clayton (-0.005)	clayton (-0.005)	clayton (-0.003)	clayton (-0.005)	clayton (0.003)	clayton (0.003)	clayton (-0.004)

Table 2: Bivariate dependencies between design variables and performance metrics, indicating the best-fit copula and rank correlation. Green color signs a positive correlation while red represents a negative correlation. Text in boldface indicates the discussed copulas.

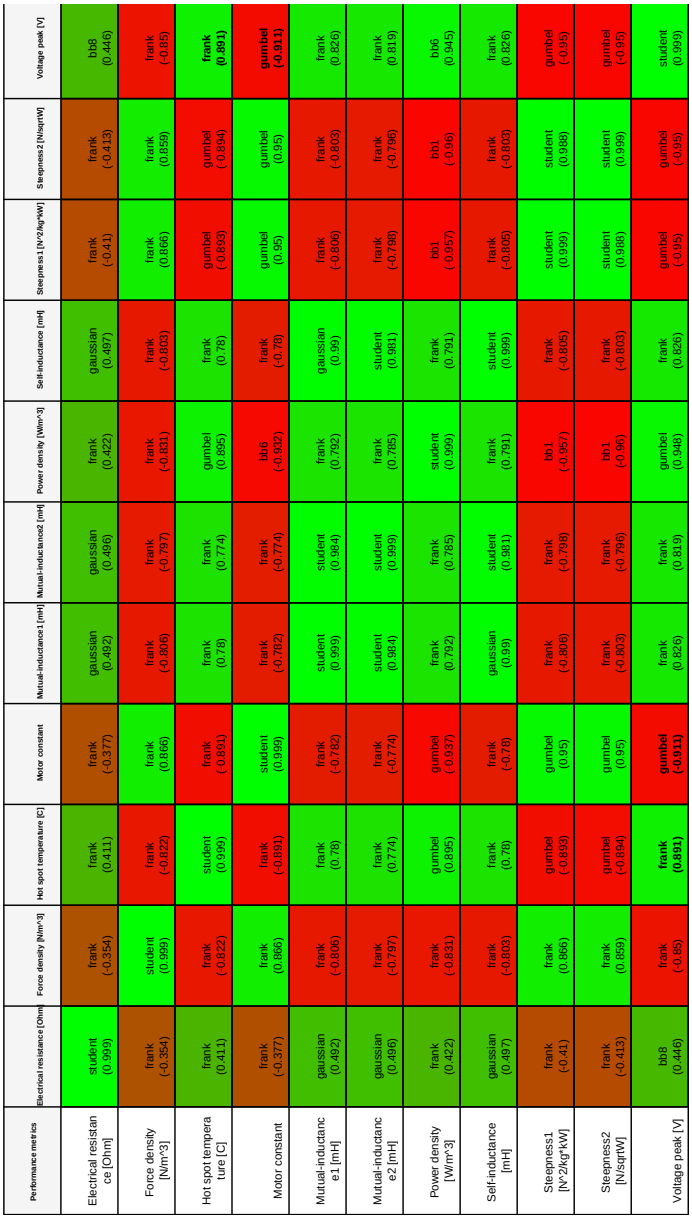

Performance metrics	Electrical resistance [Ohm]	Force density [N/m^3]	Hot spot temperature [C]	Motor constant	Mutual-inductance1 [mH]	Mutual-inductance2 [mH]	Power density [W/m^3]	Self-inductance [mH]	Steepness1 [N^2/kg*kW]	Steepness2 [N/sqrtW]	Voltage peak [V]
Electrical resistance [Ohm]	student (0.999)	frank (-0.354)	frank (0.411)	frank (-0.377)	gaussian (0.492)	gaussian (0.496)	frank (0.422)	gaussian (0.497)	frank (-0.41)	frank (-0.413)	bb8 (0.446)
Force density [N/m^3]	frank (-0.354)	student (0.999)	frank (-0.822)	frank (0.866)	frank (-0.806)	frank (-0.797)	frank (-0.831)	frank (-0.803)	frank (0.866)	frank (0.859)	frank (-0.85)
Hot spot temperature [C]	frank (0.411)	frank (-0.822)	student (0.999)	frank (-0.891)	frank (0.78)	frank (0.774)	gumbel (0.895)	frank (0.78)	gumbel (-0.893)	gumbel (-0.894)	**frank (0.891)**
Motor constant	frank (-0.377)	frank (0.866)	frank (-0.891)	student (0.999)	frank (-0.782)	frank (-0.774)	bb6 (-0.932)	frank (-0.78)	gumbel (0.95)	gumbel (0.95)	**gumbel (-0.911)**
Mutual-inductance1 [mH]	gaussian (0.492)	frank (-0.806)	frank (0.78)	frank (-0.782)	student (0.999)	student (0.984)	frank (0.792)	gaussian (0.99)	frank (-0.806)	frank (-0.803)	frank (0.826)
Mutual-inductance2 [mH]	gaussian (0.496)	frank (-0.797)	frank (0.774)	frank (-0.774)	student (0.984)	student (0.999)	frank (0.785)	student (0.981)	frank (-0.798)	frank (-0.796)	frank (0.819)
Power density [W/m^3]	frank (0.422)	frank (-0.831)	gumbel (0.895)	gumbel (-0.937)	frank (0.792)	frank (0.785)	student (0.999)	frank (0.791)	bb1 (-0.957)	bb1 (-0.96)	bb6 (0.945)
Self-inductance [mH]	gaussian (0.497)	frank (-0.803)	frank (0.78)	frank (-0.78)	gaussian (0.99)	student (0.981)	frank (0.791)	student (0.999)	frank (-0.805)	frank (-0.803)	frank (0.826)
Steepness1 [N^2/kg*kW]	frank (-0.41)	frank (0.866)	gumbel (-0.893)	gumbel (0.95)	frank (-0.806)	frank (-0.798)	bb1 (-0.957)	frank (-0.805)	student (0.999)	student (0.988)	gumbel (-0.95)
Steepness2 [N/sqrtW]	frank (-0.413)	frank (0.859)	gumbel (-0.894)	gumbel (0.95)	frank (-0.803)	frank (-0.796)	bb1 (-0.96)	frank (-0.803)	student (0.988)	student (0.999)	gumbel (-0.95)
Voltage peak [V]	bb8 (0.446)	frank (-0.85)	**frank (0.891)**	**gumbel (-0.911)**	frank (0.826)	frank (0.819)	gumbel (0.948)	frank (0.826)	gumbel (-0.95)	gumbel (-0.95)	student (0.999)

Table 3: Bivariate dependencies between performance metrics, indicating the best-fit copula and rank correlation. Green color signs a positive correlation while red represents a negative correlation. Text in boldface indicates the discussed copulas.